

Anisotropic Band Flattening in Twisted Bilayer of M-Valley MXenes

Kejie Bao,^{1,2,*} Huan Wang,^{1,2,*} Zhaochen Liu,^{1,2} and Jing Wang^{1,2,3,4,†}

¹State Key Laboratory of Surface Physics and Department of Physics, Fudan University, Shanghai 200433, China

²Shanghai Research Center for Quantum Sciences, Shanghai 201315, China

³Institute for Nanoelectronic Devices and Quantum Computing, Fudan University, Shanghai 200433, China

⁴Hefei National Laboratory, Hefei 230088, China

Experimental studies on moiré materials have predominantly focused on twisted hexagonal lattice with low-energy states near the Γ - or K-points. These materials, characterized by isotropic low-energy dispersion, are fundamentally distinct from those with anisotropic properties. Here we introduce a series of semiconducting transition metal carbides (MXenes) M_2CT_2 ($M = \text{Ti, Zr, Hf, Sc, Y}$; $T = \text{O, F, Cl}$) as a novel platform for M-valley moiré materials. Take Ti_2CO_2 and Zr_2CO_2 as representative examples, large-scale *ab initio* calculations show that their AB-stacked twisted homobilayer features three three-fold rotational symmetry related M-valleys with time-reversal symmetry and giant anisotropic band flattening. We derive a simplified moiré Hamiltonian for these systems and conduct a detailed analysis of their band structures, where the origins of anisotropic band flattening are clearly elucidated. This research broadens the scope of moiré materials, where the valley- and spin-degenerate two-dimensional array of quasi-one-dimensional system could serve as a potential platform for realizing many interesting correlated phases.

Moiré materials—synthetic two-dimensional crystals with large lattice constants resulting from the twisting of layered 2D materials—have garnered significant attention in recent years [1–5]. The flat electronic bands (compared to electron interactions) and highly tunable filling in moiré heterostructures make them an ideal platform for simulating various prototypical condensed matter systems. Notable examples include twisted bilayer graphene [6] and transition metal dichalcogenides [7, 8], which exhibit a spectrum of interacting phases such as superconductors [9–13], correlated states [14–24], Chern insulators [25–37], fractional Chern insulators [38–47] and so on [48–51].

Experimental studies on moiré materials have predominantly focused on twisted hexagonal lattice with low-energy states near the Γ - or K-points, where the low-energy dispersion is isotropic due to the three-fold rotation symmetry C_{3z} . Consequently, when band flattening occurs in moiré patterns, the bands remain dispersionless across the entire moiré Brillouin Zone (mBZ). This raises an intriguing question: what happens when the C_{3z} symmetry is significantly broken? Twisted bilayer WTe_2 offers a compelling case study, where pronounced transport anisotropy and power-law scaling of cross-wire conductance suggest the emergence of sliding Luttinger liquid upon twisting [52]. These findings indicate that anisotropic band flattening, in addition to the conventional isotropic case, is feasible in moiré systems [53–56], particularly under low-symmetry configurations. The novelty of achieving anisotropic band flattening in 2D moiré materials lies in its connection to the higher dimensional generalization of the Luttinger liquid and non Fermi liquid behavior [57–62]. This model has historically been linked to various enigmatic phases in condensed matter physics, such as the normal state of cuprate superconductors [57, 63, 64], quantum critical-

ity [65, 66] and unconventional metals [67, 68]. These insights naturally direct our attention to the underexplored M-point [53, 69] in the hexagonal lattice.

In this Letter, we present a series of semiconducting MXenes, denoted as M_2CT_2 (where $M = \text{Ti, Zr, Hf, Sc, Y}$; $T = \text{O, F, Cl}$) shown in Table I, as promising candidates for realizing M-valley moiré materials. Our findings are based on an extensive set of *ab initio* calculations, which demonstrate that anisotropic band flattening can occur in AB-stacked twisted M_2CT_2 bilayer [70]. We derive a simplified moiré Hamiltonian for these systems and conduct a detailed analysis of their band structure. Our

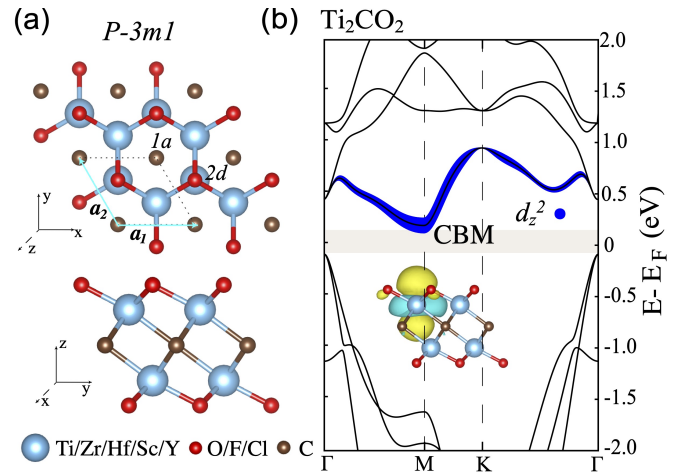


FIG. 1. (a) Structures for monolayer MXenes M_2CT_2 ($M = \text{Ti, Zr, Hf, Sc, Y}$; $T = \text{O, F, Cl}$). The Wyckoff positions $1a$ and $2d$ are displayed (notation adopted from BilbaoCrystallographic Server). (b) Band structure and band projections of d_{z^2} orbital for monolayer Ti_2CO_2 . The inner figure shows the Wannier functions predominantly contributing to CBM at M-valley.

analysis shows that the M-valley moiré Hamiltonians exhibit an emergent periodicity in the energy spectrum, which is protected by an effective symmetry (exchanging M-valley in the top and bottom layers) within the simplified model incorporating the lowest-harmonic approximation. We propose a modified mBZ that accommodates such an emergent symmetry, within which the origins of anisotropic band flattening, stemming from band folding and gap-opening processes, can be clearly elucidated.

Materials.—The monolayer MXenes (transition metal carbides) M_2CT_2 have a triangular lattice with the space group $P\bar{3}m1$ (No. 164), which includes inversion symmetry \mathcal{I} , out-of-plane three-fold rotational symmetry C_{3z} , and in-plane two-fold rotational symmetry C_{2x} . As shown in Fig. 1(a), a central carbon monolayer is sandwiched between two cation layers, and the anion layer is directly projected to the bottom cation layer on both sides. Because all d electrons of the M atoms transfer to the p orbitals of the T atoms, the ground states of these materials are spin unpolarized. Therefore, the time reversal symmetry \mathcal{T} is preserved. Their lattice constants are listed in Table I. Remarkably, these materials have already been synthesized in the experiments [71–76] and have garnered increasing attention because of their tunable band gaps [77], high carrier mobilities [78], and strong excitonic effect [79]. Taking Ti_2CO_2 as a representative example, its band structure is shown in Fig. 1(b). Notably, the conduction band minimum (CBM) is located at the M point. The Wannier functions predominantly contributing to the CBM are associated with Ti d_{z^2} orbitals. Furthermore, due to the low symmetry of the M point (with C_{2x}), the effective mass at the M-valley along the x (M-K) and y (M- Γ) directions are anisotropic, as summarized in Table I.

We then investigate the interlayer tunneling of the untwisted Ti_2CO_2 bilayer. Since monolayer Ti_2CO_2 lacks out-of-plane rotational symmetry C_{2z} , two distinct stacking configurations are considered: AA stacking, where

Materials	a (Å)	E_g (eV)	m_x (m_0)	m_y (m_0)
Ti_2CO_2	3.04	0.24	0.46	4.54
Zr_2CO_2	3.32	0.99	0.35	2.74
Hf_2CO_2	3.27	1.03	0.28	2.15
Sc_2CF_2	3.26	1.00	0.31	1.60
Y_2CF_2	3.66	1.29	0.31	1.29
Sc_2CCl_2	3.43	0.86	0.27	1.40
Y_2CCl_2	3.70	0.94	0.23	1.07

TABLE I. Lattice constant, band gap, effective mass along the x and y directions for monolayer MXenes based on GGA method [80]. The effective mass is in the unit of the free electron mass m_0 .

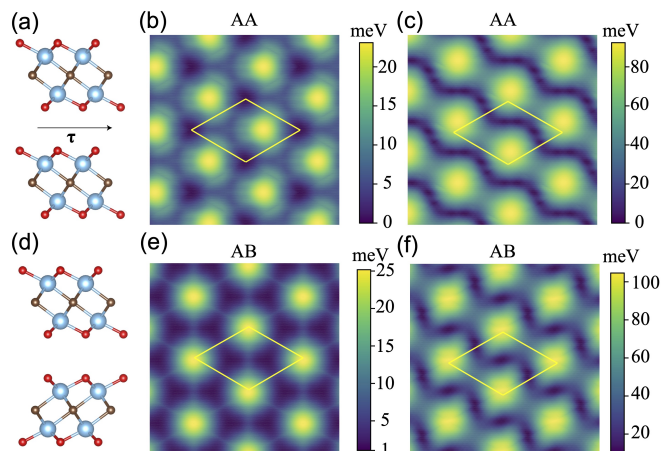


FIG. 2. (a,d): Structures of AA and AB stacking for Ti_2CO_2 with in-plane displacement $\tau = 0$. (b,e) Interlayer potential energy distribution for AA and AB stacking. (c,f) Energy splitting of M-valley at CBM for AA and AB stacking. The unit cell is illustrated by yellow lines.

the top and bottom layers are stacked directly on top of each other, and AB stacking, where the bottom layer is first rotated by 180° before stacking with the top layer, as illustrated in Fig. 2(a,d), respectively. Both AA and AB stackings share the symmetries \mathcal{I} , \mathcal{T} , and C_{3z} . However, they differ in the in-plane rotational symmetry: AA stacking exhibits C_{2x} , while AB stacking exhibits C_{2y} . We analyze the interlayer potential energy distribution for both configurations, shown in Fig. 2(b,e). The higher energy regions (bright areas) in the AA stacking configuration are denser compared to those in the AB stacking, suggesting that lattice relaxation is likely more pronounced in AA-stacked twisted bilayer. Finally, we examine the M-valley splitting for both stackings, as shown in Fig. 2(c,f), to quantify interlayer tunneling. The similarity in the patterns of M-valley splitting between the two stacking configurations indicates that their interlayer tunneling strengths are nearly identical.

M-valley moiré band.— We perform large-scale *ab initio* calculations for twisted MXenes bilayer of angle $\varphi = 3.89^\circ$, where the lattice vectors of the moiré pattern are fixed as $\mathbf{L}_i = \mathbf{a}_i \times \hat{\mathbf{z}} / (2 \sin(\varphi/2))$, and atomic relaxation is allowed [70]. In the relaxed structures, the symmetries C_{3z} , \mathcal{T} , and C_{2x} (C_{2y}) are preserved for twisted AA (AB) bilayer, while \mathcal{I} is broken. Fig. 3(c,e) display the band structures for AB-stacked twisted bilayer Ti_2CO_2 and Zr_2CO_2 , respectively. In both cases, the lowest three bands at CBM are spin degenerate and are well isolated from other bands. Notably, among these three bands, a flat band is observed along M-K and K- Γ directions, although there is noticeable dispersion along Γ -M direction. The lowest energy set of bands for Ti_2CO_2 and Zr_2CO_2 have narrow bandwidths of approximately 2.2 meV and 7.6 meV, respectively.

To elucidate the band structure from *ab initio* calculations, it is imperative to construct a moiré Hamiltonian for the M-valley in twisted bilayer systems. We begin by analyzing the electronic structure of the aligned bilayer. Since the three M-valleys are symmetrically related by C_{3z} , we can first focus on the $\eta = 0$ M-valley, as shown in Fig. 3(a). The moiré Hamiltonian for the other two M-valleys, labeled by $\eta = 1, 2$, can be derived by applying the C_{3z}^η symmetry operator. In an AB-stacked MXene homobilayer, the CBM at M-valley are predominantly characterized by d_{z^2} orbitals. These bands exhibit approximate spin $SU(2)$ symmetry due to the negligible spin-orbit coupling. Leveraging this understanding, we can now proceed to formulate the moiré Hamiltonian for the $\eta = 0$ M-valley as

$$\mathcal{H}_{\eta=0} = \begin{pmatrix} \frac{(k_x - M_x^t)^2}{2m_x} + \frac{(k_y - M_y^t)^2}{2m_y} & \Delta_T(\mathbf{r}) \\ \Delta_T^\dagger(\mathbf{r}) & \frac{(k_x - M_x^b)^2}{2m_x} + \frac{(k_y - M_y^b)^2}{2m_y} \end{pmatrix}. \quad (1)$$

The diagonal term represents the kinetic energy, where $\mathbf{M}^{t/b}$ corresponds to the momenta of the $\eta = 0$ M-valley in the top/bottom layer. The off-diagonal term describes the interlayer tunneling, which is spatially periodic with the periodicity \mathbf{L}_1 and \mathbf{L}_2 . By further considering C_{2y} and \mathcal{T} symmetries of the M-valley and applying the two-center approximation [6], we get the following form

$$\Delta_T(\mathbf{r}) = \left[t_x(1 + e^{-i\mathbf{g}_2 \cdot \mathbf{r}}) + t_y(e^{-i\mathbf{g}_1 \cdot \mathbf{r}} + e^{-i(\mathbf{g}_2 - \mathbf{g}_1) \cdot \mathbf{r}}) \right] \sigma_0. \quad (2)$$

Here we only keep the lowest-harmonic terms, t_x and t_y are real, \mathbf{g}_i denotes the moiré reciprocal lattice vectors to mBZ and $\mathbf{g}_i \cdot \mathbf{L}_j = 2\pi\delta_{ij}$, σ_0 are 2×2 identity matrix representing the spin degree of freedom, where the spin-orbital coupling effect is ignored in the interlayer tunneling.

Despite the simplicity of our moiré Hamiltonian, which is characterized by only two fitting parameters, it effectively captures the low-energy physics of the M-valley moiré system. As illustrated in Fig. 3(c,e), with the parameters $t_x = 11$ meV and $t_y = 24$ meV ($t_x = 20$ meV and $t_y = 10$ meV), the Hamiltonian accurately reproduces the lowest six bands of the twisted AB-stacked Ti_2CO_2 (Zr_2CO_2). Contributions from the three distinct M-valleys, labeled by different colors and line styles, provide a clear visualization of their individual roles in the band structure. We then investigate the energy spectrum of the lowest band within the $\eta = 0$ M-valley to gain further insights into the low-energy physics. Fig. 3(d, f) shows a pronounced quasi-1D characteristic: the electronic band exhibits significant dispersion along the x -axis, while remaining nearly flat along the y -axis. This observation highlights the anisotropic nature of the electronic structure within the M-valley.

Upon closer examination, we observe that the energy spectrum $E_{\mathbf{k}}$ exhibits periodicity along the vectors

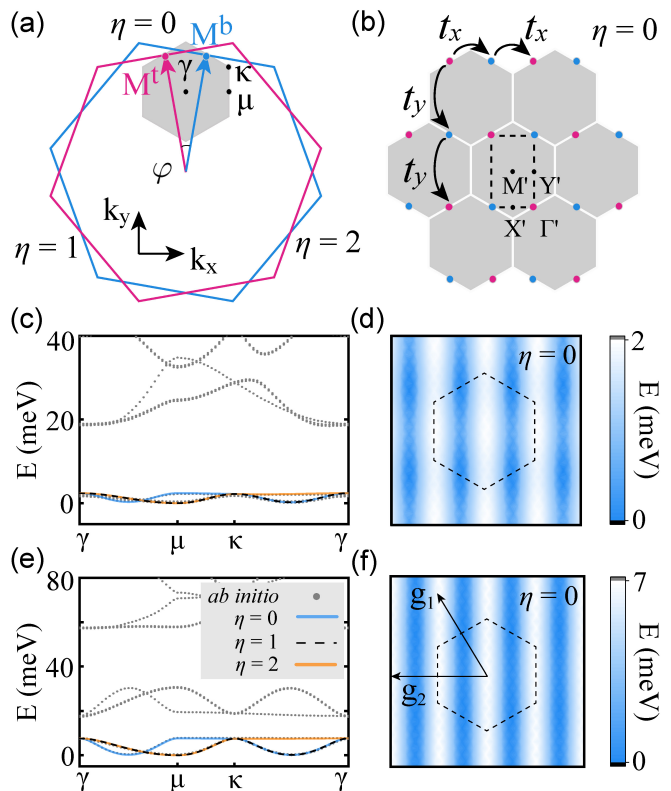


FIG. 3. (a) Monolayer BZ and moiré BZ, represented as colorful and gray hexagons, respectively. Here $\mathbf{M}^{t/b}$ labels the $\eta = 0$ M-valley in top/bottom layer, where the momentum $\mathbf{M}^t = \mathbf{g}_1/2$, $\mathbf{M}^b = (\mathbf{g}_1 - \mathbf{g}_2)/2$ in the mBZ. (b) The momentum space tight-binding model described by moiré Hamiltonian $\mathcal{H}_{\eta=0}$. Gray hexagons label the hexagonal mBZ and the dashed rectangle label the rectangle mBZ. (c,e) The band structure of twisted bilayer Ti_2CO_2 and Zr_2CO_2 at angle $\varphi = 3.89^\circ$, respectively. The results from density-functional theory are plotted as gray dot, and the fitting bands from moiré Hamiltonian \mathcal{H}_η are plotted as different color and line style according to their valley index η . (d,f) The energy spectrum of the lowest band in moiré Hamiltonian $\mathcal{H}_{\eta=0}$ with fitting parameters $t_x = 11$ meV, $t_y = 24$ meV for Ti_2CO_2 and $t_x = 20$ meV, $t_y = 10$ meV for Zr_2CO_2 .

$\mathbf{g}_2/2 = \mathbf{M}^t - \mathbf{M}^b$ and $(\mathbf{g}_2 - 2\mathbf{g}_1)/2 = -\mathbf{M}^t - \mathbf{M}^b$, a feature prominently displayed in Fig. 3(d). This periodicity is attributed to the emergent symmetry inherent in our simplified moiré Hamiltonian $\mathcal{H}_{\eta=0}$. The Hamiltonian effectively represents a tight-binding model in reciprocal space, where the hopping integrals between momentum states \mathbf{M}^t and \mathbf{M}^b along the x and y directions are denoted by t_x and t_y , respectively. As depicted in Fig. 3(b), the moiré Hamiltonian $\mathcal{H}_{\eta=0}$ is invariant under the exchange of \mathbf{M}^t and \mathbf{M}^b combined with the momentum space translation along $\mathbf{g}_2/2$ or $(\mathbf{g}_2 - 2\mathbf{g}_1)/2$, which imparts the energy spectrum with the observed periodicity: $E_{\mathbf{k}} = E_{\mathbf{k}+\mathbf{g}_2/2} = E_{\mathbf{k}+(\mathbf{g}_2-2\mathbf{g}_1)/2}$. This phenomenon aligns with the effective M_z symmetry described in Ref. [81].

This symmetry plays a pivotal role in shaping the electronic structure of the M-valley moiré system, underscoring the significance of the simple yet profound moiré Hamiltonian in capturing the essential physics of the system. It should be noted that emergent symmetry is typically compromised when higher harmonic terms are taken into account. While these terms are negligible in twisted AB-stacked Ti_2CO_2 and Zr_2CO_2 bilayer, they become significant in their twisted AA-stacked counterparts [70].

Anisotropic band flattening at M-valley.— Given that the emergent periodicity in the energy spectrum $E_{\mathbf{k}}$ originates from the effective symmetry of exchanging M-valley between layers, we can find the conventional hexagonal mBZ is deemed redundant for the context of band structure analysis. Therefore, we adopt a rectangular mBZ that better reflects the reduced symmetry characteristic of the M-valley. Specifically, the reciprocal lattice vectors to the rectangular mBZ is $\mathbf{g}_2/2$ and $(\mathbf{g}_2 - 2\mathbf{g}_1)/2$. The boundaries of the rectangular mBZ are marked by dashed lines in Fig. 2(b), clearly illustrating the modified mBZ that accommodates the emergent symmetry in the moiré Hamiltonian.

Using the rectangular mBZ, we can now elucidate the construction of the quasi-1D bands within the M-valley. For this analysis, we set the parameters to $\varphi = 4^\circ$, lattice constant $a = 3 \text{ \AA}$, $m_x = 2m_0$, and $m_y = 0.3m_0$. With these parameters, we compute the moiré band structure for varying values of t_x and t_y , and present the results in both the hexagonal and rectangular mBZ, as shown in Fig. 4. In the case where $t_x = t_y = 0 \text{ meV}$, the band structure reveals that all bands touch at the mBZ boundary, a result of band folding due to the absence of the moiré potential. Within the rectangular mBZ, we find that the bandwidth of the lowest band in the $\eta = 0$ M-valley is 20 meV along the Γ' - X' direction and 10 meV along the Γ' - Y' direction. These differences in bandwidth are attributed to the distinct mass terms and the dimensions of the rectangular mBZ along each axis.

When setting $t_x = 20 \text{ meV}$ and $t_y = 5 \text{ meV}$, as illustrated in the right column of Fig. 4(b), gaps open at the high-symmetry points X' and Y' , with magnitudes approximately equal to twice the respective hopping parameters, i.e., 40 meV and 10 meV. This gap-opening process effectively isolates the lowest band from the higher-energy bands, resulting in a topologically trivial anisotropic band within each M-valley. The scenario becomes particularly intriguing when $t_x = 5 \text{ meV}$ and $t_y = 20 \text{ meV}$. Similar to the previous case, the gaps at X' and Y' are approximately twice the values of t_x and t_y , respectively. However, in this configuration, the bandwidth along the Γ' - Y' direction is significantly smaller than t_y , leading to the formation of a nearly flat band along the y direction as shown in Fig. 4(c). This phenomenon aligns with the observations in twisted bilayer Ti_2CO_2 and Zr_2CO_2 . Interestingly, anisotropic band flattening along the x direction is also feasible, albeit it requires a

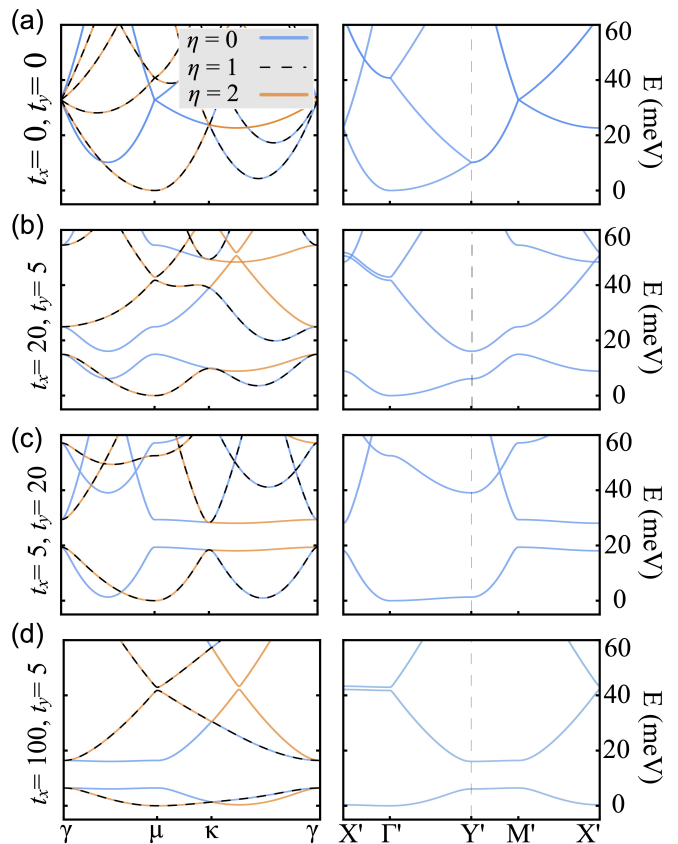


FIG. 4. The band structure from moiré Hamiltonian Eq. (1) with typical t_x, t_y parameters plotted in the hexagonal (left column) and rectangular mBZ (right column). The different line color and style label the contribution from different M-valleys in hexagonal mBZ, while in rectangular mBZ only the $\eta = 0$ M-valley is plotted. Here we set $\varphi = 4^\circ$, lattice constant $a = 3 \text{ \AA}$, $m_x = 0.3m_0$, $m_y = 2m_0$. (a) $t_x = t_y = 0 \text{ meV}$. (b) $t_x = 20 \text{ meV}$, $t_y = 5 \text{ meV}$. (c) $t_x = 5 \text{ meV}$, $t_y = 20 \text{ meV}$. (d) $t_x = 100 \text{ meV}$, $t_y = 5 \text{ meV}$.

substantially larger t_x to overcome the bandwidth along the Γ' - X' direction. As demonstrated in the right column of Fig. 4(d), using parameters $t_x = 100 \text{ meV}$ and $t_y = 5 \text{ meV}$, we observe a flat band along the x direction. This configuration corresponds to the case observed in twisted AA-stacked SnSe_2 , as calculated in Ref. [81].

From the preceding discussion, now it is clear that the anisotropic band flattening observed in the lowest band of the M-valley can be understood through the mechanisms of band folding and gap opening around the M-point. This phenomenon resembles the anisotropic band flattening in the Γ -valley moiré system such as twisted bilayer black phosphorus, as we calculated previously [55]. The key distinction between the two systems lies in the multiplicity of the valleys: the M-valley exhibits a three-fold degeneracy, while the Γ -valley has no valley degeneracy.

Discussions.— We have introduced a series of semiconducting MXenes, with Ti_2CO_2 and Zr_2CO_2 as paradig-

matic examples, as a promising and novel platform for M-valley moiré materials. The presence of three C_{3z} -related valleys and anisotropic band flattening makes M-point moiré materials manifestly different from Γ - and K-point twisted hexagonal systems. By constructing the corresponding moiré Hamiltonians, we have revealed that the mechanism underlying the anisotropic band flattening is attributed to the band folding and gap opening processes around M-points. The direction of anisotropic band flattening is not determined by symmetry but interlayer tunneling parameters, which is different from the initial proposal in Ref. [53].

This C_{3z} -related 2D array of quasi-1D systems may serve as a tunable platform for realizing the crossed sliding Luttinger liquid [82–84] and investigating non-Fermi liquid behavior. In addition, the current system resembles the previously studied p -orbital physics in cubic and square lattices. Extending earlier exact results on itinerant ferromagnetism to this system could yield valuable insights into the phenomena [85, 86]. Under strong interactions and in the anisotropic limit, the combination of perfect nesting and the frustrated nature of the triangular lattice could result in a rich interplay of spin, charge, and valley density waves [87–89]. Furthermore, at integer fillings and within the Mott insulating regime, the underlying spin-valley exchange interactions may reveal novel spin-valley physics. For instance, the coupled-wire construction, previously employed to study exotic 2D spin liquid [90], offers a compelling framework, together with our system serving as an excellent platform for exploring such phenomena.

This work is supported by the Natural Science Foundation of China through Grants No. 12350404 and No. 12174066, the Innovation Program for Quantum Science and Technology through Grant No. 2021ZD0302600, the Science and Technology Commission of Shanghai Municipality under Grants No. 23JC1400600, No. 24LZ1400100 and No. 2019SHZDZX01.

Note added. During the finalization of our manuscript, we become aware of related works on a similar topic [81, 91]. These studies also introduced M-valley moiré materials, but they differ from our work in terms of material proposals and theoretical analysis. Similar conclusions are reached wherever there is overlap.

* These authors contribute equally to the work.

† wjingphys@fudan.edu.cn

- [1] E. Y. Andrei, D. K. Efetov, P. Jarillo-Herrero, A. H. MacDonald, K. F. Mak, T. Senthil, E. Tutuc, A. Yazdani, and A. F. Young, The marvels of moiré materials, *Nature Rev. Mater.* **6**, 201 (2021).
- [2] D. M. Kennes, M. Claassen, L. Xian, A. Georges, A. J. Millis, J. Hone, C. R. Dean, D. N. Basov, and A. N. Pasupathy, Moiré heterostructures as a condensed-matter quantum simulator, *Nature Phys.* **17**, 155 (2021).
- [3] L. Balents, C. R. Dean, D. K. Efetov, and A. F. Young, Superconductivity and strong correlations in moiré flat bands, *Nature Phys.* **16**, 725 (2020).
- [4] S. Carr, S. Fang, and E. Kaxiras, Electronic-structure methods for twisted moiré layers, *Nature Rev. Mater.* **5**, 748 (2020).
- [5] K. F. Mak and J. Shan, Moiré heterostructures as a condensed-matter quantum simulator, *Nature Nanotechnol.* **17**, 686 (2022).
- [6] R. Bistritzer and A. H. MacDonald, Moiré bands in twisted double-layer graphene, *Proc. Natl. Acad. Sci. U.S.A.* **108**, 12233 (2011).
- [7] F. Wu, T. Lovorn, E. Tutuc, and A. H. MacDonald, Hubbard model physics in transition metal dichalcogenide moiré bands, *Phys. Rev. Lett.* **121**, 026402 (2018).
- [8] F. Wu, T. Lovorn, E. Tutuc, I. Martin, and A. H. MacDonald, Topological insulators in twisted transition metal dichalcogenide homobilayers, *Phys. Rev. Lett.* **122**, 086402 (2019).
- [9] Y. Cao, V. Fatemi, S. Fang, K. Watanabe, T. Taniguchi, E. Kaxiras, and P. Jarillo-Herrero, Unconventional superconductivity in magic-angle graphene superlattices, *Nature* **556**, 43 (2018).
- [10] M. Yankowitz, S. Chen, H. Polshyn, Y. Zhang, K. Watanabe, T. Taniguchi, D. Graf, A. F. Young, and C. R. Dean, Tuning superconductivity in twisted bilayer graphene, *Science* **363**, 1059 (2019).
- [11] B. Lian, Z. Wang, and B. A. Bernevig, Twisted bilayer graphene: A phonon-driven superconductor, *Phys. Rev. Lett.* **122**, 257002 (2019).
- [12] Y. Xia, Z. Han, K. Watanabe, T. Taniguchi, J. Shan, and K. F. Mak, Superconductivity in twisted bilayer wse₂, *Nature* 10.1038/s41586-024-08116-2 (2024).
- [13] Y. Guo, J. Pack, J. Swann, L. Holtzman, M. Cothrine, K. Watanabe, T. Taniguchi, D. Mandrus, K. Barmak, J. Hone, A. J. Millis, A. N. Pasupathy, and C. R. Dean, Superconductivity in twisted bilayer wse₂ (2024), [arXiv:2406.03418](https://arxiv.org/abs/2406.03418) [cond-mat.mes-hall].
- [14] Y. Cao, V. Fatemi, A. Demir, S. Fang, S. L. Tomarken, J. Y. Luo, J. D. Sanchez-Yamagishi, K. Watanabe, T. Taniguchi, E. Kaxiras, R. C. Ashoori, and P. Jarillo-Herrero, Correlated insulator behaviour at half-filling in magic-angle graphene superlattices, *Nature* **556**, 80 (2018).
- [15] X. Lu, P. Stepanov, W. Yang, M. Xie, M. A. Aamir, I. Das, C. Urgell, K. Watanabe, T. Taniguchi, G. Zhang, A. Bachtold, A. H. MacDonald, and D. K. Efetov, Superconductors, orbital magnets and correlated states in magic-angle bilayer graphene, *Nature* **574**, 653 (2019).
- [16] Z.-D. Song and B. A. Bernevig, Magic-angle twisted bilayer graphene as a topological heavy fermion problem, *Phys. Rev. Lett.* **129**, 047601 (2022).
- [17] A. Kerelsky, L. J. McGilly, D. M. Kennes, L. Xian, M. Yankowitz, S. Chen, K. Watanabe, T. Taniguchi, J. Hone, C. Dean, A. Rubio, and A. N. Pasupathy, Maximized electron interactions at the magic angle in twisted bilayer graphene, *Nature* **572**, 95 (2019).
- [18] Y.-Z. Chou and S. Das Sarma, Kondo lattice model in magic-angle twisted bilayer graphene, *Phys. Rev. Lett.* **131**, 026501 (2023).
- [19] Z. Zhu, S. Carr, D. Massatt, M. Luskin, and E. Kaxiras, Twisted trilayer graphene: A precisely tunable platform for correlated electrons, *Phys. Rev. Lett.* **125**, 116404

- (2020).
- [20] Y. Tang, L. Li, T. Li, Y. Xu, S. Liu, K. Barmak, K. Watanabe, T. Taniguchi, A. H. MacDonald, J. Shan, and K. F. Mak, Simulation of hubbard model physics in wse_2/ws_2 moiré superlattices, *Nature* **579**, 353 (2020).
- [21] M. Claassen, L. Xian, D. M. Kennes, and A. Rubio, Ultra-strong spin-orbit coupling and topological moiré engineering in twisted wse_2 bilayers, *Nature Commun.* **13**, 4915 (2022).
- [22] D. N. Sheng, A. P. Reddy, A. Abouelkomsan, E. J. Bergholtz, and L. Fu, Quantum anomalous hall crystal at fractional filling of moiré superlattices, *Phys. Rev. Lett.* **133**, 066601 (2024).
- [23] L. Wang, E.-M. Shih, A. Ghiotto, L. Xian, D. A. Rhodes, C. Tan, M. Claassen, D. M. Kennes, Y. Bai, B. Kim, K. Watanabe, T. Taniguchi, X. Zhu, J. Hone, A. Rubio, A. N. Pasupathy, and C. R. Dean, Correlated electronic phases in twisted bilayer transition metal dichalcogenides, *Nature Mater.* **19**, 861 (2020).
- [24] E. Anderson, F.-R. Fan, J. Cai, W. Holtzmann, T. Taniguchi, K. Watanabe, D. Xiao, W. Yao, and X. Xu, Programming correlated magnetic states with gate-controlled moiré geometry, *Science* **381**, 325 (2023).
- [25] A. L. Sharpe, E. J. Fox, A. W. Barnard, J. Finney, K. Watanabe, T. Taniguchi, M. A. Kastner, and D. Goldhaber-Gordon, Emergent ferromagnetism near three-quarters filling in twisted bilayer graphene, *Science* **365**, 605 (2019).
- [26] M. Serlin, C. L. Tschirhart, H. Polshyn, Y. Zhang, J. Zhu, K. Watanabe, T. Taniguchi, L. Balents, and A. F. Young, Intrinsic quantized anomalous hall effect in a moiré heterostructure, *Science* **367**, 900 (2020).
- [27] G. Chen, A. L. Sharpe, E. J. Fox, Y.-H. Zhang, S. Wang, L. Jiang, B. Lyu, H. Li, K. Watanabe, T. Taniguchi, Z. Shi, T. Senthil, D. Goldhaber-Gordon, Y. Zhang, and F. Wang, Tunable correlated chern insulator and ferromagnetism in a moiré superlattice, *Nature Nanotechnol.* **579**, 56 (2020).
- [28] K. P. Nuckolls, M. Oh, D. Wong, B. Lian, K. Watanabe, T. Taniguchi, B. A. Bernevig, and A. Yazdani, Strongly correlated chern insulators in magic-angle twisted bilayer graphene, *Nature* **588**, 610 (2020).
- [29] F. Wu and S. Das Sarma, Collective excitations of quantum anomalous hall ferromagnets in twisted bilayer graphene, *Phys. Rev. Lett.* **124**, 046403 (2020).
- [30] Z. Dong, A. S. Patri, and T. Senthil, Theory of quantum anomalous hall phases in pentalayer rhombohedral graphene moiré structures, *Phys. Rev. Lett.* **133**, 206502 (2024).
- [31] G. Tarnopolsky, A. J. Kruchkov, and A. Vishwanath, Origin of magic angles in twisted bilayer graphene, *Phys. Rev. Lett.* **122**, 106405 (2019).
- [32] T. Li, S. Jiang, B. Shen, Y. Zhang, L. Li, Z. Tao, T. Devakul, K. Watanabe, T. Taniguchi, L. Fu, J. Shan, and K. F. Mak, Quantum anomalous hall effect from intertwined moiré bands, *Nature* **600**, 641 (2021).
- [33] T. Devakul, V. Crépel, Y. Zhang, and L. Fu, Magic in twisted transition metal dichalcogenide bilayers, *Nature Commun.* **12**, 6730 (2021).
- [34] M. Angeli and A. H. MacDonald, Γ valley transition metal dichalcogenide moiré bands, *Proc. Natl. Acad. Sci. U.S.A.* **118**, e2021826118 (2021).
- [35] Z. Liu, H. Wang, and J. Wang, Magnetic moiré surface states and flat chern bands in topological insulators, *Phys. Rev. B* **106**, 035114 (2022).
- [36] B. A. Foutty, C. R. Kometter, T. Devakul, A. P. Reddy, K. Watanabe, T. Taniguchi, L. Fu, and B. E. Feldman, Mapping twist-tuned multiband topology in bilayer wse_2 , *Science* **384**, 343 (2024).
- [37] X.-W. Zhang, C. Wang, X. Liu, Y. Fan, T. Cao, and D. Xiao, Polarization-driven band topology evolution in twisted $mote_2$ and wse_2 , *Nature Commun.* **15**, 4223 (2024).
- [38] Z. Lu, T. Han, Y. Yao, A. P. Reddy, J. Yang, J. Seo, K. Watanabe, T. Taniguchi, L. Fu, and L. Ju, Fractional quantum anomalous hall effect in multilayer graphene, *Nature* **626**, 759 (2024).
- [39] J. Herzog-Arbeitman, Y. Wang, J. Liu, P. M. Tam, Z. Qi, Y. Jia, D. K. Efetov, O. Vafek, N. Regnault, H. Weng, Q. Wu, B. A. Bernevig, and J. Yu, Moiré fractional chern insulators. ii. first-principles calculations and continuum models of rhombohedral graphene superlattices, *Phys. Rev. B* **109**, 205122 (2024).
- [40] F. Xu, Z. Sun, T. Jia, C. Liu, C. Xu, C. Li, Y. Gu, K. Watanabe, T. Taniguchi, B. Tong, J. Jia, Z. Shi, S. Jiang, Y. Zhang, X. Liu, and T. Li, Observation of integer and fractional quantum anomalous hall effects in twisted bilayer $mote_2$, *Phys. Rev. X* **13**, 031037 (2023).
- [41] H. Park, J. Cai, E. Anderson, Y. Zhang, J. Zhu, X. Liu, C. Wang, W. Holtzmann, C. Hu, Z. Liu, T. Taniguchi, K. Watanabe, J.-H. Chu, T. Cao, L. Fu, W. Yao, C.-Z. Chang, D. Cobden, D. Xiao, and X. Xu, Observation of fractionally quantized anomalous hall effect, *Nature* **622**, 74 (2023).
- [42] Y. Zeng, Z. Xia, K. Kang, J. Zhu, P. Knüppel, C. Vaswani, K. Watanabe, T. Taniguchi, K. F. Mak, and J. Shan, Thermodynamic evidence of fractional chern insulator in moiré $mote_2$, *Nature* **622**, 69 (2023).
- [43] J. Cai, E. Anderson, C. Wang, X. Zhang, X. Liu, W. Holtzmann, Y. Zhang, F. Fan, T. Taniguchi, K. Watanabe, Y. Ran, T. Cao, L. Fu, D. Xiao, W. Yao, and X. Xu, Signatures of fractional quantum anomalous hall states in twisted $mote_2$, *Nature* **622**, 63 (2023).
- [44] C. Wang, X.-W. Zhang, X. Liu, Y. He, X. Xu, Y. Ran, T. Cao, and D. Xiao, Fractional chern insulator in twisted bilayer $mote_2$, *Phys. Rev. Lett.* **132**, 036501 (2024).
- [45] Y. Jia, J. Yu, J. Liu, J. Herzog-Arbeitman, Z. Qi, H. Pi, N. Regnault, H. Weng, B. A. Bernevig, and Q. Wu, Moiré fractional chern insulators. i. first-principles calculations and continuum models of twisted bilayer $mote_2$, *Phys. Rev. B* **109**, 205121 (2024).
- [46] J. Yu, J. Herzog-Arbeitman, M. Wang, O. Vafek, B. A. Bernevig, and N. Regnault, Fractional chern insulators versus nonmagnetic states in twisted bilayer $mote_2$, *Phys. Rev. B* **109**, 045147 (2024).
- [47] H. Li, Y. Su, Y. B. Kim, H.-Y. Kee, K. Sun, and S.-Z. Lin, Contrasting twisted bilayer graphene and transition metal dichalcogenides for fractional chern insulators: An emergent gauge picture, *Phys. Rev. B* **109**, 245131 (2024).
- [48] A. Kerelsky, L. J. McGilly, D. M. Kennes, L. Xian, M. Yankowitz, S. Chen, K. Watanabe, T. Taniguchi, J. Hone, C. Dean, A. Rubio, and A. N. Pasupathy, Isospin pomeranchuk effect in twisted bilayer graphene, *Nature* **592**, 220 (2021).
- [49] M. Huang, Z. Wu, X. Zhang, X. Feng, Z. Zhou, S. Wang, Y. Chen, C. Cheng, K. Sun, Z. Y. Meng, and N. Wang, Intrinsic nonlinear hall effect and gate-switchable berry

- curvature sliding in twisted bilayer graphene, *Phys. Rev. Lett.* **131**, 066301 (2023).
- [50] H. Yoo, R. Engelke, S. Carr, S. Fang, K. Zhang, P. Cazeaux, S. H. Sung, R. Hovden, A. W. Tsen, T. Taniguchi, K. Watanabe, G.-C. Yi, M. Kim, M. Lusk, E. B. Tadmor, E. Kaxiras, and P. Kim, Atomic and electronic reconstruction at the van der waals interface in twisted bilayer graphene, *Nature Mater.* **18**, 448 (2019).
- [51] D. Halbertal, N. R. Finney, S. S. Sunku, A. Kerelsky, C. Rubio-Verdú, S. Shabani, L. Xian, S. Carr, S. Chen, C. Zhang, L. Wang, D. Gonzalez-Acevedo, A. S. McLeod, D. Rhodes, K. Watanabe, T. Taniguchi, E. Kaxiras, C. R. Dean, J. C. Hone, A. N. Pasupathy, D. M. Kennes, A. Rubio, and D. N. Basov, Moiré metrology of energy landscapes in van der waals heterostructures, *Nature Commun.* **12**, 242 (2021).
- [52] P. Wang, G. Yu, Y. H. Kwan, Y. Jia, S. Lei, S. Klemen, F. A. Cevallos, R. Singha, T. Devakul, K. Watanabe, T. Taniguchi, S. L. Sondhi, R. J. Cava, L. M. Schoop, S. A. Parameswaran, and S. Wu, One-dimensional luttinger liquids in a two-dimensional moiré lattice, *Nature* **605**, 57 (2022).
- [53] T. Kariyado and A. Vishwanath, Flat band in twisted bilayer bravais lattices, *Phys. Rev. Res.* **1**, 033076 (2019).
- [54] D. M. Kennes, L. Xian, M. Claassen, and A. Rubio, One-dimensional flat bands in twisted bilayer germanium selenide, *Nature Commun.* **11**, 1124 (2019).
- [55] H. Wang, Z. Liu, Y. Jiang, and J. Wang, Giant anisotropic band flattening in twisted Γ -valley semiconductor bilayers, *Phys. Rev. B* **108**, L201120 (2023).
- [56] Y. Hu, Y. Xu, and B. Lian, Twisted coupled wire model for a moiré sliding luttinger liquid, *Phys. Rev. B* **110**, L201106 (2024).
- [57] P. W. Anderson, Hall effect in the two-dimensional luttinger liquid, *Phys. Rev. Lett.* **67**, 2092 (1991).
- [58] V. J. Emery, E. Fradkin, S. A. Kivelson, and T. C. Lubensky, Quantum theory of the smectic metal state in stripe phases, *Phys. Rev. Lett.* **85**, 2160 (2000).
- [59] R. Mukhopadhyay, C. L. Kane, and T. C. Lubensky, Sliding luttinger liquid phases, *Phys. Rev. B* **64**, 045120 (2001).
- [60] A. Vishwanath and D. Carpentier, Two-dimensional anisotropic non-fermi-liquid phase of coupled luttinger liquids, *Phys. Rev. Lett.* **86**, 676 (2001).
- [61] S. L. Sondhi and K. Yang, Sliding phases via magnetic fields, *Phys. Rev. B* **63**, 054430 (2001).
- [62] Y.-M. Wu, C. Murthy, and S. A. Kivelson, Possible sliding regimes in twisted bilayer wte_2 , *Phys. Rev. Lett.* **133**, 246501 (2024).
- [63] P. W. Anderson, “luttinger-liquid” behavior of the normal metallic state of the 2d hubbard model, *Phys. Rev. Lett.* **64**, 1839 (1990).
- [64] B. Wuyts, E. Osquiguil, M. Maenhoudt, S. Libbrecht, Z. X. Gao, and Y. Bruynseraede, Influence of the oxygen content on the normal-state hall angle in $yba_2cu_3O_{x-m}$ films, *Phys. Rev. B* **47**, 5512 (1993).
- [65] L. Classen, I. Zaliznyak, and A. M. Tsvelik, Three-dimensional non-fermi-liquid behavior from one-dimensional quantum critical local moments, *Phys. Rev. Lett.* **120**, 156404 (2018).
- [66] B. Lake, D. A. Tennant, C. D. Frost, and S. E. Nagler, Quantum criticality and universal scaling of a quantum antiferromagnet, *Nature Mater.* **4**, 329 (2005).
- [67] H.-C. Jiang, M. S. Block, R. V. Mishmash, J. R. Garrison, D. N. Sheng, O. I. Motrunich, and M. P. A. Fisher, Non-fermi-liquid d-wave metal phase of strongly interacting electrons, *Nature* **493**, 39 (2013).
- [68] I. Khait, P. Azaria, C. Hubig, U. Schollwöck, and A. Auerbach, Doped kondo chain, a heavy luttinger liquid, *Proc. Natl. Acad. Sci. U.S.A.* **115**, 5140 (2018).
- [69] T. Kariyado, Twisted bilayer bc_3 : Valley interlocked anisotropic flat bands, *Phys. Rev. B* **107**, 085127 (2023).
- [70] See Supplemental Material for methods and technical details.
- [71] M. Naguib, O. Mashtalir, J. Carle, V. Presser, J. Lu, L. Hultman, Y. Gogotsi, and M. W. Barsoum, Two-dimensional transition metal carbides, *ACS Nano* **6**, 1322 (2012).
- [72] S. Lai, J. Jeon, S. K. Jang, J. Xu, Y. J. Choi, J.-H. Park, E. Hwang, and S. Lee, Surface group modification and carrier transport properties of layered transition metal carbides (Ti_2CT_x , T:—OH,—F, and —O), *Nanoscale* **7**, 19390 (2015).
- [73] S. A. Melchior, K. Raju, I. S. Ike, R. M. Erasmus, G. Kabongo, I. Sigalas, S. E. Iyuke, and K. I. Ozoemena, High-voltage symmetric supercapacitor based on 2d titanium carbide (mxene, Ti_2CT_x)/carbon nanosphere composites in a neutral aqueous electrolyte, *J. Electrochem. Soc.* **165**, A501 (2018).
- [74] D. Wang, C. Zhou, A. S. Filatov, W. Cho, F. Lagunas, M. Wang, S. Vaikuntanathan, C. Liu, R. F. Klie, and D. V. Talapin, Direct synthesis and chemical vapor deposition of 2d carbide and nitride mxenes, *Science* **379**, 1242 (2023).
- [75] D. L. Druffel, M. G. Lanetti, J. D. Sundberg, J. T. Pawlik, M. S. Stark, C. L. Donley, L. M. McRae, K. M. Scott, and S. C. Warren, Synthesis and electronic structure of a 3d crystalline stack of mxene-like sheets, *Chem. Mater.* **31**, 9788 (2019).
- [76] S. J. Hwu, R. P. Ziebarth, S. Von Winbush, J. E. Ford, and J. D. Corbett, Synthesis and structure of double-metal-layered scandium, yttrium, and zirconium chloride carbides and nitrides, M_2Cl_2C and M_2Cl_2N , *Inorg. Chem.* **25**, 283 (1986).
- [77] Y. Zhang, W. Xia, Y. Wu, and P. Zhang, Prediction of mxene based 2D tunable band gap semiconductors: GW quasiparticle calculations, *Nanoscale* **11**, 3993 (2019).
- [78] X. Zhang, X. Zhao, D. Wu, Y. Jing, and Z. Zhou, High and anisotropic carrier mobility in experimentally possible Ti_2CO_2 (mxene) monolayers and nanoribbons, *Nanoscale* **7**, 16020 (2015).
- [79] S. Dong and Y. Li, Robust high-temperature topological excitonic insulator of transition-metal carbide mxenes, *Phys. Rev. B* **107**, 235147 (2023).
- [80] J. P. Perdew, K. Burke, and M. Ernzerhof, Generalized gradient approximation made simple, *Phys. Rev. Lett.* **77**, 3865 (1996).
- [81] D. Călugăru, Y. Jiang, H. Hu, H. Pi, J. Yu, M. G. Vergniory, J. Shan, C. Felser, L. M. Schoop, D. K. Efetov, K. F. Mak, and B. A. Bernevig, A new moiré platform based on m-point twisting (2024), arXiv:2411.18684 [cond-mat.str-el].
- [82] R. Mukhopadhyay, C. L. Kane, and T. C. Lubensky, Crossed sliding luttinger liquid phase, *Phys. Rev. B* **63**, 081103 (2001).
- [83] B. Gao, A. Komnik, R. Egger, D. C. Glatli, and A. Bachtold, Evidence for luttinger-liquid behavior in crossed

- metallic single-wall nanotubes, *Phys. Rev. Lett.* **92**, 216804 (2004).
- [84] X. Du, L. Kang, Y. Lv, J. Zhou, X. Gu, R. Xu, Q. Zhang, Z. Yin, W. Zhao, Y. Li, *et al.*, Crossed luttinger liquid hidden in a quasi-two-dimensional material, *Nature Phys.* **19**, 40 (2023).
- [85] Y. Li, E. H. Lieb, and C. Wu, Exact results for itinerant ferromagnetism in multiorbital systems on square and cubic lattices, *Phys. Rev. Lett.* **112**, 217201 (2014).
- [86] Y. Li, Exact results for itinerant ferromagnetism in a t_{2g} -orbital system on cubic and square lattices, *Phys. Rev. B* **91**, 115122 (2015).
- [87] E. Zhao and W. V. Liu, Orbital order in mott insulators of spinless p -band fermions, *Phys. Rev. Lett.* **100**, 160403 (2008).
- [88] Z. Zhang, X. Li, and W. V. Liu, Stripe, checkerboard, and liquid-crystal ordering from anisotropic p -orbital fermi surfaces in optical lattices, *Phys. Rev. A* **85**, 053606 (2012).
- [89] E. Fradkin, S. A. Kivelson, and J. M. Tranquada, Colloquium: Theory of intertwined orders in high temperature superconductors, *Rev. Mod. Phys.* **87**, 457 (2015).
- [90] R. G. Pereira and S. Bieri, Gapless chiral spin liquid from coupled chains on the kagome lattice, *SciPost Phys.* **4**, 004 (2018).
- [91] C. Lei, P. T. Mahon, and A. H. MacDonald, Moiré band theory for m-valley twisted transition metal dichalcogenides (2024), arXiv:2411.18828 [cond-mat.mes-hall].